Atmos. Chem. Phys. Discuss., 15, 35547–35589, 2015
www.atmos-chem-phys-discuss.net/15/35547/2015/
doi:10.5194/acpd-15-35547-2015

Atmospheric Chemistry and Physics Discussions

Summertime sources of dimethyl sulfide in the Canadian Arctic Archipelago and Baffin Bay

E. L. Mungall[1], B. Croft[2], M. Lizotte[3], J. L. Thomas[4], J. G. Murphy[1], M. Levasseur[3], R. V. Martin[2], J. J. B. Wentzell[5], J. Liggio[5], and J. P. D. Abbatt[1]

[1]Department of Chemistry, University of Toronto, Toronto, Canada
[2]Department of Physics and Atmospheric Science, Dalhousie University, Halifax, Canada
[3]Québec-Océan, Department of Biology, Université Laval, Québec, Canada
[4]Sorbonne Universités, UPMC Univ. Paris 06, Université Versailles St-Quentin, CNRS/INSU, LATMOS-IPSL, Paris, France
[5]Air Quality Processes Research Section, Environment Canada, Toronto, Ontario, Canada

Received: 1 December 2015 – Accepted: 4 December 2015 – Published: 16 December 2015

Correspondence to: J. Abbatt (jabbatt@chem.utoronto.ca)

Published by Copernicus Publications on behalf of the European Geosciences Union.

Abstract

Dimethyl sulfide (DMS) plays a major role in the global sulfur cycle. In addition, its atmospheric oxidation products contribute to the formation and growth of atmospheric aerosol particles, thereby influencing cloud condensation nuclei (CCN) populations and thus cloud formation. The pristine summertime Arctic atmosphere is a CCN-limited regime, and is thus very susceptible to the influence of DMS. However, atmospheric DMS mixing ratios have only rarely been measured in the summertime Arctic. During July–August 2014, we conducted the first high time resolution (10 Hz) DMS mixing ratio measurements for the Eastern Canadian Archipelago and Baffin Bay as one component of the Network on Climate and Aerosols: Addressing Key Uncertainties in Remote Canadian Environments (NETCARE). DMS mixing ratios ranged from below the detection limit of 4 to 1155 pptv (median 186 pptv). A set of transfer velocity parameterizations from the literature coupled with our atmospheric and coincident seawater DMS measurements yielded air-sea DMS flux estimates ranging from 0.02–12 $\mu mol\,m^{-2}\,d^{-1}$, the first published for this region in summer. Airmass trajectory analysis using FLEXPART-WRF and chemical transport modeling using GEOS-Chem indicated that local sources (Lancaster Sound and Baffin Bay) were the dominant contributors to the DMS measured along the 21 day ship track, with episodic transport from the Hudson Bay System. After adjusting GEOS-Chem oceanic DMS values in the region to match measurements, GEOS-Chem reproduced the major features of the measured time series, but remained biased low overall (median 67 pptv). We investigated non-marine sources that might contribute to this bias, such as DMS emissions from lakes, biomass burning, melt ponds and coastal tundra. While the local marine sources of DMS dominated overall, our results suggest that non-local and possibly non-marine sources episodically contributed strongly to the observed summertime Arctic DMS mixing ratios.

ACPD
15, 35547–35589, 2015

1 Introduction

Despite the established importance of oceanic emissions of biogenic sulfur in the form of dimethyl sulfide (DMS) to aerosol formation and growth in the marine boundary layer (e.g. Charlson et al., 1987; Leaitch et al., 2013), key uncertainties remain about oceanic DMS concentrations and the air-sea flux of DMS (Tesdal et al., 2015). DMS emissions are responsible for about 15 % of the tropospheric sulfur budget globally, and up to 100 % in the most remote areas (Bates et al., 1992). DMS is relatively insoluble, so after being produced by micro-organisms in surface waters it escapes to the atmosphere where it is oxidized to sulfuric acid and methane sulfonic acid (MSA). These oxidation products can then participate in new particle formation (Pirjola et al., 1999; Chen et al., 2015) or condense upon existing particles, causing them to grow larger. The influence of DMS emissions on aerosol concentrations is important since aerosols modify the climate directly by scattering and absorbing radiation, and indirectly by modifying cloud radiative properties by acting as seeds for cloud droplet formation (Charlson et al., 1987; Twomey, 1977; Albrecht, 1989). Both composition and size affect the ability of an aerosol particle to act as a cloud condensation nucleus (CCN), with bigger and more water soluble aerosol particles preferentially activating as CCN. The condensation of the water-soluble products of DMS oxidation on atmospheric aerosol particles thus makes them better CCN through both the composition and size effects.

Through a combination of limited local sources and efficient scavenging mechanisms (Browse et al., 2012) the summer Arctic atmosphere contains very few CCN. At low CCN levels the radiative balance as determined by cloud cover is very sensitive to CCN number. Sea ice cover in the summer Arctic is in rapid decline (e.g. Tilling et al., 2015). With the decline in sea ice comes an enhanced potential for sea–air exchange of compounds such as DMS that may affect aerosol populations in the Arctic. In general, increased numbers of CCN are associated with a cooling effect on climate. However, since the Arctic can reside in a CCN-limited cloud-aerosol regime an increase in CCN could have a warming effect on the summer Arctic as an increase in cloudiness could

ACPD
15, 35547–35589, 2015

be associated with increased trapping of outgoing radiation (Mauritsen et al., 2011). In order to predict future changes in CCN number, we need to understand the influence of sea–air exchange on aerosols in the summer Arctic.

Quantifying present-day atmospheric DMS (henceforth referred to as DMS_g) provides an important benchmark for interpreting future measurements. Currently, only a few snapshots of DMS_g in the Arctic exist from a handful of ship-board studies conducted over the last twenty years, none of which captured the most biologically productive time of June and July (Leck and Persson, 1996; Rempillo et al., 2011; Chang et al., 2011; Tjernström et al., 2014). The data span great distances in time and space and provide only a fragmented picture of tropospheric DMS levels in the Arctic. Understanding present-day sources of DMS is also relevant for predicting how these sources may change in a future climate. The goals of this study are (1) to present ship-board DMS_g measurements taken in the Canadian Arctic during July and August 2014, and (2) to identify sources for the measured DMS_g.

The intermediate lifetime of DMS_g against OH oxidation of 1–2 days means that whether it travels far before being oxidized or remains in the same area depends strongly on atmospheric transport patterns. Atmospheric transport mixes DMS_g within the region, effectively smoothing out atmospheric concentration inhomogeneities due to inhomogeneity in the surface water DMS (referred to henceforth as DMS_{sw}). Transport can also bring DMS_g from regions further afield. For example, a study by Nilsson and Leck (2002) highlighted the importance of transport in bringing DMS_g from regions of open water to regions covered by sea ice within the Arctic.

Despite the potential for an important role for atmospheric transport, few source apportionment studies for sulfur in the Arctic have been carried out. Previous work has focused almost exclusively on the aerosol phase. A common assumption that all methane sulfonic acid (MSA) in the aerosol phase arises from oxidation of marine biogenic DMS_g (Sharma et al., 2012). However, Hopke et al. (1995) suggested that terrestrial sources in Northern Canada could also contribute MSA to Arctic aerosol. Previous studies indicate that terrestrial emissions of DMS_g from soils, vegetation, wet-

ACPD
15, 35547–35589, 2015

lands and lakes are less important than oceanic emissions (Bates et al., 1992; Watts, 2000). However, these studies are based on very few or even no measurements in the Canadian North, and the fluxes for the Canadian tundra and boreal forest, which cover a very large surface area, are highly unconstrained. Much of the Arctic Ocean is in close proximity to land and is more subject to terrestrial influence than the open ocean in other regions of the world (Macdonald et al., 2015).

Sources of DMS_g other than seawater are not typically included in chemical transport and climate models, despite evidence in the literature for several other sources of DMS_g. For example, significant levels of DMS have been measured in Canadian lakes (Sharma et al., 1999a; Richards et al., 1994). DMS emissions have also been observed from various continental sources such as lichens (Gries et al., 1994), crops such as corn (Bates et al., 1992), wetlands (Nriagu et al., 1987), and biomass burning (Meinardi et al., 2003; Akagi et al., 2011). Terrestrial plants can be an important source of DMS as demonstrated by DMS levels in the hundreds of pptv range measured from creosote bush in Arizona and from trees and soils in the Amazonian rain forest (Jardine et al., 2010, 2014). One previous study based on sulfur isotopes from Greenland included pooled biogenic continental and volcanic sources (as their isotopic signatures are not easily distinguishable) and estimated this continental component to be 44 % (Patris et al., 2002). In addition to the possibility of a continental source, melt ponds have been suggested as a potentially important source of DMS to the atmosphere (Levasseur, 2013). These fresh or brackish ponds form from snow melt on top of the sea ice in spring and summer, and have been observed to have an extremely large areal extent, covering 30 % of the sea ice on average in midsummer with up to 90 % coverage in some regions (Rosel and Kaleschke, 2012). Here we present sensitivity studies to examine the potential importance of these alternative sources of DMS_g.

Section 2 outlines our measurement methodology. Section 3 presents the measured DMS_g time series along 3 weeks of the cruise. Section 3 also includes concurrent measurements of DMS_{sw} and the calculated DMS air-sea flux estimates for the region. We use the GEOS-Chem chemical transport model and the FLEXPART-WRF particle

ACPD
15, 35547–35589, 2015

dispersion model to interpret these measurements. Section 4 includes an examination of source regions for the measured DMS_g and sensitivity studies related to possible terrestrial sources.

2 Methods

2.1 Measurements

Measurements of DMS were made during the first leg of the CCGS Amundsen summer campaign under the aegis of NETCARE (Network on Climate and Aerosols: Addressing Uncertainties in Remote Canadian Environments). The research cruise started in Quebec City on 8 July 2014 and ended in Kugluktuk on 14 August 2014. Measurements were made in Baffin Bay, Lancaster Sound and Nares Strait. The ship track is shown in Fig. 1a.

2.1.1 DMS mixing ratios

DMS_g measurements were made using a high resolution time of flight chemical ionization mass spectrometer (HR-ToF-CIMS, Aerodyne). The instrument was housed in a container on the foredeck. The inlet was placed on a tower 9.44 m above the deck at the bow, which was itself nominally 6.6 m a.s.l. (in total ca. 16 m a.s.l.). A diaphragm pump pulled air at 30 standard L min^{-1} through a 25 m long, 9.53 mm inner diameter PFA line heated to 50 °C (Clayborn Labs). Flow rate through the line was controlled by a critical orifice. The flow was subsampled and pulled to the instrument inlet through another critical orifice restricting the flow to 2 standard L min^{-1}. The flow through the sealed ^{210}Po source of the HR-ToF-CIMS, also controlled at 2 standard L min^{-1} by a critical orifice, was supplied by a zero air generator (Parker Balston, Model HPZA-18000, followed by a Carbon Scrubber P/N B06-0263) via a mass flow controller supplying 2.4 standard L min^{-1}. The zero air generator also supplied 9.8 sccm (controlled by a mass flow controller) through a bubbler filled with benzene, which was added to

ACPD
15, 35547–35589, 2015

the flow through the radioactive source to provide the reagent ion. The excess went to exhaust. Figure S1 in the Supplement shows a flow schematic.

The use of benzene cations as a reagent ion for chemical ionization mass spectrometry was first proposed by Allgood et al. (1990). This reagent ion was successfully applied to the shipboard detection of DMS by the group of Tim Bertram at UCSD (Kim et al., 2015). The ionization mechanism that prevails is the transfer of charge from a benzene cation to an analyte ion which has an ionization energy lower than that of benzene (Allgood et al., 1990). Due to space constraints on board the ship, a zero air generator was used instead of cylinder nitrogen to produce our reagent ion flows. The use of zero air introduced other potential reagent ions to the mass spectrum (O_2^+, NO^+, $C_6H_7^+$, and $H_2O \cdot H_3O^+$, shown in Fig. S2 in the Supplement). To investigate the effect of this more complicated reagent ion source, calibration experiments were carried out in the laboratory prior to the campaign for both air and N_2 at different sample flow relative humidities and under different CIMS voltage configurations. The calibration curves for DMS (detected as $CH_3SCH_3^+$) showed a linear response under all conditions. We found that the sensitivity of the instrument to DMS did not depend on relative humidity, and for operating conditions in the field averaged about 80 cps pptv^{-1} with detection limits below 4 pptv due to the background being in the 2–3 pptv range.

Background spectra were collected in the field by overflowing the inlet with zero air from the zero air generator as shown in Fig. S1. The high mass resolution of the instrument eliminated concern about isobaric interferences as indicated in Fig. S3 in the Supplement. Mass spectra were collected at 10 Hz. One point calibrations were performed nearly every day by overflowing the inlet with zero air and adding a known amount of DMS from a standards cylinder using a mass flow controller (499 ± 5 % ppb, Apel-Reimer). Peak fitting was performed using the Tofware software package from Aerodyne (version 2.4.4) in Igor Pro. Reported mixing ratios were calculated by first normalizing analyte peak areas to reagent ion peak areas, then subtracting backgrounds, and finally applying calibration factors obtained by linearly interpolating the one-point daily calibrations. Text S1 in the Supplement provides details. The data were

ACPD
15, 35547–35589, 2015

filtered such that values were removed when the ship was moving (speed over ground greater than 2 m s^{-1}) and the wind direction was not within ±90° of the bow. This was intended to remove artifacts that might have occurred due to enhanced DMS flux in the ship's wake. This removed less than 12 % of data points.

2.1.2 Surface seawater DMS concentrations

Seawater concentrations of DMS were determined following procedures described by Scarratt et al. (2000) and modified in Lizotte et al. (2012) using purging, cryotrapping and sulfur-specific gas chromatography. Briefly, seawater was gently collected directly from 12 L Niskin bottles in gas-tight 24 mL serum vials, allowing the water to overflow. Subsamples of DMS were withdrawn from the 24 mL serum vials within minutes of collection and sparged using an in line purge and trap system with a Varian 3800 gas chromatograph (GC) equipped with a pulsed flame photometric detector (PFPD). The GC was calibrated with injections of a 100 nM solution of hydrolyzed DMSP (Research Plus Inc.). The full dataset will be presented separately (M. Lizotte et al., personal communication, 2015).

2.1.3 Meteorological data

Basic meteorological measurements were made from a purpose built tower on the ship's foredeck. Air temperature (8.2 m above deck), wind speed and direction (9.4 m above deck) and barometric pressure (1.5 m above deck) were measured using, respectively, a shielded temperature and relative humidity probe (Vaisala™HMP45C212), wind monitor (RM Young 05103) and pressure transducer (RM Young™61205V). Sensors were scanned every 2 s and saved as 2 min averages to a micrologger (Campbell Scientific™model CR3000). Platform relative wind was post-processed to true wind following Smith et al. (1999). Navigation data (ship position, speed over ground, course over ground and heading) necessary for the conversion were available from the ship's position and orientation system (Applanix POS MV™V4). Periods when the tower sen-

ACPD
15, 35547–35589, 2015

sors were serviced or when the platform relative wind was beyond ±90° from the ship's bow were screened from the meteorological data set. Screened periods accounted for less than 20 % of total data but up to 45 % in some regions.

2.1.4 Sea surface temperature and salinity

Sea surface temperature (SST) was measured with the ship's Inboard Shiptrack Water System, Seabird/Seapoint measurement system. There were no continuous salinity measurements. An average salinity value of 29.7 PSU was used for all calculations since the calculated transfer velocities had very low sensitivity to changes in salinity for our study region.

2.2 Modeling

2.2.1 FLEXPART-WRF

A Lagrangian particle dispersion model based on FLEXPART (Stohl et al., 2005), FLEXPART-WRF (Brioude et al., 2013, website: flexpart.eu/wiki/FpLimitedareaWrf), was used to study the origin of air sampled by the ship. The model is driven by meteorology from the Weather Research and Forecasting (WRF) Model (Skamarock et al., 2005) and was run in backward mode to study the emissions source regions and transport pathways influencing ship-based DMS measurements. Specific details are in another publication arising from the NETCARE Amundsen campaign (Wentworth et al., 2015).

2.2.2 GEOS-Chem

The GEOS-Chem chemical transport model (http://www.geos-chem.org) was used to interpret the atmospheric measurements. We used GEOS-Chem version 9-02 at $2^\circ \times 2.5^\circ$ resolution with 47 vertical layers between the surface and 0.01 hPa. The assimilated meteorology is taken from the National Aeronautics and Space Administra-

ACPD
15, 35547–35589, 2015

tion (NASA) Global Modeling and Assimilation Office (GMAO) Goddard Earth Observing System version 5.7.2 (GEOS-FP) assimilated meteorology product, which includes both hourly surface fields and 3 hourly 3-D fields. Our simulations used 2014 meteorology and allowed a 2 month spin-up prior to the simulation of July and August 2014.

The GEOS-Chem model includes a detailed oxidant-aerosol tropospheric chemistry mechanism as originally described by Bey et al. (2001). Simulated aerosol species include sulphate-nitrate-ammonium (Park et al., 2004, 2006), carbonaceous aerosols (Park et al., 2003; Liao et al., 2007), dust (Fairlie et al., 2007, 2010) and sea salt (Alexander et al., 2005). The sulphate-nitrate-ammonium chemistry uses the ISORROPIA II thermodynamic model (Fountoukis and Nenes, 2007), which partitions ammonia and nitric acid between the gas and aerosol phases. The model includes natural and anthropogenic sources of SO_2 and NH_3 (Fisher et al., 2011b). DMS emissions are based on the Liss and Merlivat (1986) sea–air flux formulation and oceanic DMS concentrations from Lana et al. (2011). In our simulations, DMS emissions occurred only in the fraction of the grid box that is covered by sea water and also free of sea ice. Biomass burning emissions are from the Quick Fire Emissions Dataset (QFED2) (Darmenov and da Silva, 2013), which provides daily open fire emissions at $0.1^\circ \times 0.1^\circ$. Oxidation of SO_2 occurs in clouds by reaction with H_2O_2 and O_3 and in the gas phase with OH (Alexander et al., 2009) and DMS oxidation occurs by reaction with OH and NO_3.

The GEOS-Chem model has been extensively applied to study the Arctic including for aerosol acidity (Wentworth et al., 2015; Fisher et al., 2011a), carbonaceous aerosol (Wang et al., 2011), aerosol number (Croft et al., 2015), aerosol absorption (Breider et al., 2014), and mercury (Fisher et al., 2012).

2.2.3 Seawater DMS values in GEOS-Chem

The DMS_{sw} values used in the standard GEOS-Chem are monthly means from the climatology of Lana et al. (2011), which was developed based on very few data points in the Canadian Arctic Archipelago and Baffin Bay. The Lana et al. (2011) climatology

ACPD
15, 35547–35589, 2015

predicts values of DMS_{sw} below 5 nM in this region, while the values measured on board the ship during the campaign were often between 5–10 nM and occasionally higher. Therefore, we used the measured values as input in GEOS-Chem in lieu of the Lana et al. (2011) values for the study region. The measured values were interpolated using the DIVA web application (http://gher-diva.phys.ulg.ac.be/web-vis/diva.html) and a static field was used for July and August.

To our knowledge, there exist no measurements of DMS_{sw} in the Hudson Bay System (comprising Hudson Bay, Foxe Basin and the Hudson Strait; referred to as HBS hereafter). In order the assess the potential importance of this source region to DMS_g further north, we used primary productivity as a proxy for DMS_{sw} for lack of better options. To the best of our knowledge, no accepted proxy for DMS_{sw} exists, and the development of such a proxy, while extremely valuable, is beyond the scope of this work. The work of Ferland et al. (2011) found that the waters of Hudson Strait are as productive as those of the North Water (Northern Baffin Bay), while Hudson Bay and Foxe Basin are about a quarter as productive. For our simulation we set the DMS_{sw} in Hudson Strait to be equal to that measured in the North Water, and the DMS_{sw} in Hudson Bay and Foxe Basin to a quarter of that value. The values chosen here for DMS_{sw} represent what we believe to be a plausible scenario. In the absence of measurements, it is not possible to further constrain what the DMS_{sw} values might be in the Hudson Bay System.

2.3 Flux estimate calculations

Concurrent measurements of DMS in the atmosphere and seawater along the ship track allow us to estimate the air-sea flux of DMS. The flux is defined as the rate of transfer of a gas across a surface, in this case the surface of the ocean. For liquid-gas surfaces, the flux is described by Eq. (1),

$$F = -K_W \left(C_g/K_H - C_l\right) \quad (1)$$

ACPD
15, 35547–35589, 2015

where C_g and C_l are the concentrations of the chemical species of interest in the gas phase and liquid phase respectively, K_W is the transfer velocity, and K_H is the dimensionless gas over liquid form of the Henry's law constant (Johnson, 2010). The transfer velocity K_W is described by Eq. (2),

$$K_W = \left[\frac{1}{k_a} + \frac{K_H}{k_w}\right]^{-1} \quad (2)$$

where K_W is composed of the single phase transfer velocities for both the water-side (k_w) and the air-side (k_a), representing the rates of transfer in each phase.

The transfer velocity for each phase encapsulates the physical processes controlling the flux in that phase. For soluble gases, the air-side processes play a more important role, and become increasingly relevant with increasing solubility, while insoluble gases exhibit exclusively water-side control (Wanninkhof et al., 2009). Air-sea fluxes are controlled by many different factors, which has led to the development of a proliferation of transfer velocity parameterizations, each addressing different issues. Some are physically based, i.e. attempt to mathematically describe the processes at play, while others are developed by fitting experimental or field data. It is not clear whether parameterizations developed based on measurements of the flux of a given gas can be applied to other gases. For example, bubbles contribute less to the DMS flux than they do to the CO_2 flux, due to the limited solubility of carbon dioxide in water, and so parameterizations developed for CO_2 might be expected to overestimate the DMS flux (Blomquist et al., 2006).

We used multiple transfer velocity parameterizations from the literature together with our measurements of atmospheric DMS mixing ratios, seawater DMS concentrations and wind speed to calculate fluxes. We compared these parameterizations to attempt to clarify the impact of the choice of parameterization on calculated fluxes. These parameterizations are summarized in Table 1 and are referred to by acronyms of the form FXY (F for flux), where X represents the air-side transfer velocity and Y represents the water-side transfer velocity. Thus, for example, the transfer velocity parameteri-

ACPD
15, 35547–35589, 2015

zation using the air-side parameterization of Jeffery et al. (2010) and the water-side parameterization of Liss and Merlivat (1986) is referred to as FJLM. The acronyms referring to the various parameterizations are listed in Table 1. Johnson implemented a wide variety (Table 1 provides details) of both air-side and water-side parameterizations (Johnson, 2010), all of which require only wind speed, air temperature, and salinity as inputs. The relationship of the transfer velocity arising from each parameterization with wind speed for the conditions encountered during the cruise is shown in Fig. S4 in the Supplement. Loose et al. (2014) recently published a parameterization specific to the seasonal ice zone, incorporating ice-specific physical processes. This parameterization was used to calculate the water-side transfer velocity whenever the ship was in the marginal ice zone, using estimated sea ice coverage and ice speeds.

Sea ice cover near the ship's location was estimated at a $0.5^{\circ} \times 0.5^{\circ}$ resolution by plotting the ship's course at hourly resolution on daily ice charts obtained from the Canadian Ice Service (http://www.ec.gc.ca/glaces-ice/). These estimates were cross-referenced with daily photos taken aboard the ship to ensure accuracy. Estimates were made on a scale from 1–10, with no fractional values. Ice speed was estimated using the relationship to wind speed found by (Cole et al., 2014), $u_{\mathrm{ice}} = 0.019\, u_{\mathrm{air}}$.

Fluxes were calculated according to Eq. (1) as the transfer velocity multiplied by the difference in concentration between the atmosphere and the ocean. Atmospheric concentrations were calculated from measured mixing ratios using measured atmospheric temperature and pressure and divided by the Henry's law constant for DMS at the in situ temperature. Fluxes estimated by all transfer velocity parameterizations that did not explicitly include the effect of sea ice were multiplied by the fraction of open water in order to account for the capping effect of sea ice (Loose et al., 2014).

3 DMS mixing ratio observations and estimated fluxes

Figure 1b and Table 2 present the DMS_g mixing ratio data collected along the ship track. These are the first published DMS_g values for the Arctic during midsummer

ACPD
15, 35547–35589, 2015

(July). These summertime measurements exceed previous measurements made in late summer and early fall by a factor of 3–10 (Table 2). This is consistent with the expectation of higher biological productivity in the summer than in other seasons (Levasseur, 2013). The time series shows high temporal variability. In particular, three episodes of elevated DMS_g mixing ratios with values of 400 pptv or above occurred along the ship track on 18–20 July, 26 July and 1–2 August. Two episodes of much lower DMS_g mixing ratios with values below 100 pptv occurred on 22–23 July and 5 August. Comparing these measurements to those made in other regions of the world ocean indicates that our values are on the same order (hundreds of pptv) as measurements made at high latitudes under bloom conditions in the Southern Ocean (Bell et al., 2015), the North Atlantic (Bell et al., 2013), and the North West Pacific (Tanimoto et al., 2013), but are higher than measurements made in the Tropical Pacific which were on the order of tens of pptv (Simpson et al., 2014).

Figure 2 presents the time series of DMS along the ship track together with the other variables needed to estimate fluxes (wind speed and seawater DMS concentrations) and shows the flux estimates as a time series for each transfer velocity parameterization used. Figure 3 shows the regional median DMS air-sea fluxes based on the ship track measurements for the Eastern Canadian Arctic summer. Previous DMS flux estimates for the Arctic are summarized in Table 3. The only other summertime estimate falls within the same range as in this work of ca. 0–10 $\mu mol\,day^{-1}\,m^{-2}$ (Sharma et al., 1999b). Our values may represent an underestimate of the true regional flux, as wind speeds were low at the times when the highest DMS_{sw} values were observed on 23 and 31 July. It is probable that these high-DMS_{sw} regions experienced higher wind speeds at other times, leading to a larger flux. A better constrained summer flux estimate for this region will require sampling of DMS_{sw} at higher spatial and temporal resolution, and ideally direct continuous flux measurements using a technique such as eddy covariance, but these are challenging measurements rendered more so by the remoteness of Arctic Ocean.

ACPD
15, 35547–35589, 2015

Figures 2 and 3 show that the choice of transfer velocity parameterization had little impact on the calculated fluxes the majority of the time, with the exception being times at which wind speeds were high (greater than 10 $m\,s^{-1}$) during the period of 18–19 July. In particular, the choice of air-side parameterization (the difference between FLL, FLD, FLMY, FLS and FLJ in Fig. 3) had very little impact on the estimated fluxes, as shown by the similarity of the medians and distributions of the fluxes estimated using these different parameterizations. Without direct flux measurements, we cannot determine which water-side transfer velocity parameterization is the most accurate. However, recent studies have shown that the wind speed dependence of the DMS transfer velocity is close to linear (Huebert et al., 2010; Bell et al., 2013, 2015). As a result we chose to use a linear dependence of transfer velocity on wind speed in our GEOS-Chem simulations following the Liss and Merlivat (1986) parameterization.

Ultimately, more data is needed in order to evaluate which transfer velocity parameterization is most suited to modeling DMS fluxes, and whether this varies geographically. For example, the FJLo parameterization, which explicitly includes the effects of sea ice in the marginal ice zone, predicts fluxes a factor of 2 larger than the other parameterizations do. This serves as a hint that accounting for the effect of sea ice on air-sea exchange in models (beyond a simple capping effect) may be important to modeling emissions of climatologically active gases such as DMS. Even without the additional consideration of regional differences such as sea ice cover, considerable uncertainty concerning transfer velocity parameterizations remains. It is probable that all of the factors controlling air-sea flux are not yet understood (Johnson et al., 2011), and would in any case be very difficult to model. Accurate parameterization of sea–air fluxes is an active area of research, and advances in the field are essential to chemical transport models.

ACPD
15, 35547–35589, 2015

4 Source apportionment with GEOS-Chem and FLEXPART

In order to explore the provenance of the air masses being sampled on the ship, we used FLEXPART-WRF backward runs as well as GEOS-Chem simulations. Figure 4 summarizes our understanding of the origins of air masses arriving at the ship track. Figure 4a shows the time series of DMS_g from the GEOS-Chem simulation superimposed on the measured DMS_g time series, as well as the GEOS-Chem sea salt (a marine tracer) and methyl ethyl ketone and carbon monoxide (MEK and CO, biomass burning tracers) mixing ratios. Figure 4b shows the main land cover types in the region. Panel c in Fig. 4 shows examples of potential emissions sensitivity plots generated using FLEXPART-WRF that indicate regions the air has passed over before being sampled. Periods highlighted with a gray bar and numbered 1 through 3 were chosen as representative of three types of influence: (1) marine influence from south of the Arctic circle, (2) terrestrial influence from Northern Canada, and (3) regional marine influence from Baffin Bay. Sea salt tracer maxima indicate marine-influenced air and reflect high winds, while MEK and CO maxima indicate an influence from biomass burning. Biomass burning tracers provide a convenient indication of continental influence on the airmass. Figure 4 shows agreement between the sources of the air indicated by FLEXPART-WRF and by the GEOS-Chem tracers. For example, during Period 2 the MEK tracer is high and FLEXPART-WRF shows continental influence, while during Period 3 the sea salt tracer is high and FLEXPART-WRF shows marine influence.

4.1 Model-measurement comparison

Our GEOS-Chem simulations reproduce the major features of the measured DMS_g time series, with appropriate magnitudes much of the time and an overall bias of −67 pptv. The poorest model-measurement agreements occur on 1–2 and 6–7 August, as shown in Figs. 5b and 4a, where GEOS-Chem overestimates DMS mixing ratios by a factor of 2–3. This overestimation coincides with high levels of the accumulation mode sea salt aerosol tracer in GEOS-Chem as shown in Fig. 4b. The overestimation may be

ACPD
15, 35547–35589, 2015

due to the DMS_{sw} values for that time period being too large (given our use of a static field based on only a few measurements), to excessive GEOS wind speeds driving too large of a flux during this episode, or to errors in the parameterization used for the transfer velocity at high wind speeds. Wind speeds in our GEOS-Chem simulations are generally within a factor of 2 of the observed wind speeds along the ship track time series. Overall, GEOS-Chem tended to overestimate DMS_g in Baffin Bay (largely open water at the time of the campaign) and underestimate it in Lancaster Sound (where we encountered between 10–100 % ice cover). It is worth noting that the effect of sea ice on sea–air flux as hypothesized by Loose et al. (2014) is to increase the flux at low wind speeds and decrease it at high wind speeds. Implementation of this transfer velocity parameterization might be expected to improve model-measurement agreement.

4.2 Local sources: Baffin Bay and Lancaster Sound

Figure 5a shows the relative contributions of various marine source regions to the GEOS-Chem simulation of the DMS_g along the ship track. Nearly 90 % of the simulated DMS was contributed by the areas the ship was traveling through, Baffin Bay and Lancaster Sound (shown in blue and purple respectively). These local emissions also contributed the majority of the highest mixing ratios observed during the campaign on 18 and 20 July. Overall, the waters of Baffin Bay and Lancaster Sound acted as a strong local source of DMS_g throughout the campaign.

4.3 Transport: role of Hudson Bay System

Figure 5 shows that the influence of the HBS is significant on 18–19 July, contributing up to 60 % of simulated DMS_g over that time period. This peak in DMS coincided with a storm originating in lower latitudes blowing through Lancaster Sound, where the ship was located at the time. This transport pattern is visible in the FLEXPART-WRF retroplume for Period 1 in Fig. 4c. These results suggest that DMS emissions from the HBS have the potential to be an important source of atmospheric sulfur to the Arctic atmo-

ACPD
15, 35547–35589, 2015

sphere during episodic transport events associated with mid latitude storms traveling northward. This result depends on the assumption that the DMS_{sw} values in the HBS are similar to levels observed at higher latitudes. However, the potential for influence from the HBS is supported by previous reports of high levels of DMS in air masses transported northward from the Hudson Bay region (Sjostedt et al., 2012). Measurements of both DMS_{sw} and DMS_g in the HBS are needed to confirm this hypothesis.

4.4 Investigation of possible missing sources

The GEOS-Chem simulated DMS_g time series fails to reproduce the peak in measured DMS_g on 26 July (shown in Fig. 4a). This mismatch coincides with a minimum in the simulated marine tracer (sea salt), suggesting that a non-marine source of DMS_g is not being represented in the model. We expect DMS_g and the sea salt tracer to covary in the model as their emissions are similarly dependent on wind speed and fraction of open ocean and their lifetimes are similarly short. It is possible that this disagreement indicates that the model does not capture the true relationship of DMS_g to wind speed. However, the FLEXPART-WRF retroplumes for 26 July (an example is shown as Period 2 of Fig. 4c) indicate that the airmass had not traveled over very much open water before reaching the ship's location. This is supported by high levels of continental tracers (e.g. MEK, shown in the third panel of Fig. 4a) during these same periods.

The suggestion that DMS_g may have a continental source is not new (Hopke et al., 1995), but it has not received very much attention. The FLEXPART-WRF PES retroplumes indicate that the continental area influencing the air masses sampled by the ship was Northern Canada (primarily, regions to the south and est of Baffin Bay, including Nunavut and the Northwest Territories). The land cover in that region is shown in Fig. 4b and is a mixture of tundra, boreal forest, wetlands and lakes. As well, there was a wide spatial extent of melt ponds to the south and west of the ship track (shown in Fig. S5 in the Supplement). To assess the impact each of these sources may have had on the DMS_g measured during the campaign, we estimated the DMS emission potential of each land cover type (including melt ponds) using published values where

ACPD
15, 35547–35589, 2015

possible. We implemented these extra emissions in the GEOS-Chem model and performed sensitivity tests to explore their potential contributions to DMS_g at the ship positions. These results are presented in the following subsections.

4.4.1 Emissions from melt ponds

Melt ponds form on the surface of sea ice as the snow melts. They cover much of the surface of the sea ice by mid summer and have been suggested as a potentially important source of DMS to the atmosphere (Levasseur, 2013). At the time of the campaign, the sea ice regions to the west and south of our ship track, particularly in Lancaster Sound, had considerable melt pond coverage as shown in Fig. S5. The melt pond DMS source was implemented in GEOS-Chem by assuming that 50 % of sea ice was covered by melt ponds and treating melt ponds as seawater in the model, that is, using the same flux parameterization as for open ocean (Liss and Merlivat, 1986). The validity of assuming the same flux parameterization applies to a shallow melt pond as to the open ocean is untested, but as discussed previously, the uncertainties associated with parameterizing transfer velocities in general are quite large, so we consider this approximation reasonable for our sensitivity test. The concentration of DMS_{sw} in the melt ponds was set to 3 nM. This value was chosen to provide a reasonable upper limit based on measurements by Levasseur (2013).

The blue curve in Fig. 5c shows the modeled DMS contributed by the melt pond source. The melt pond contribution to the simulated DMS_g time series at the ship track was greatest during 18–25 July when the ship was in Lancaster Sound. The melt ponds contributed a maximum of 100 % to the total simulated DMS_g at the ship position on 23 July when modeled and measured DMS_g were very low. The strong contribution of the melt ponds at this time was likely due to the ship's position at the ice edge and advection of the arriving airmass over ice-covered regions. The simulated melt pond source contributed an average of close to 20 % of the total simulated DMS_g over the remainder of the time series. Addition of this source reduced the overall normalized mean model bias by 9 %, suggesting that melt ponds could serve to elevate the regional

ACPD
15, 35547–35589, 2015

background levels of DMS_g. More measurements of DMS concentrations in melt ponds and, ideally, direct measurements of DMS fluxes from melt ponds will further constrain the impact this source might have on DMS_g in the Arctic summer.

4.4.2 Emissions from coastal tundra

Previous studies suggest that DMS emissions from lichens (Gries et al., 1994) and from coastal tundra, particularly in regions where snow geese breed (Hines and Morrison, 1992), may be quite large. For lichens to emit reduced sulfur to the atmosphere, they require a source of sulfur. In coastal regions this can be supplied by sea spray. We implemented a tundra DMS source in GEOS-Chem by using the Olson Land Cover data (http://edc2.usgs.gov/glcc/globdoc2_0.php) to calculate the fraction of each GEOS-Chem grid box covered by the land type "barren tundra". We then assumed that 40 % of that tundra (to account for inland regions emitting less due to less sulfate being deposited by sea spray) emitted DMS at a rate of 480 $nM\,m^{-2}\,h^{-1}$ (Hines and Morrison, 1992). We consider this simulation to give us an upper limit to the potential influence of tundra DMS emissions.

The results are presented as the brown curve in Fig. 5c. The simulated DMS_g at the ship track had the largest contribution from tundra sources during 16–17 July, with a maximum contribution to the simulated DMS_g at the ship position of 6 %. The percent contribution was lower than that of the melt pond source because the tundra source acted to increase simulated DMS_g during times when levels were already high, but as can be seen in Fig. 5c the absolute contribution of the modeled tundra source was comparable to or larger than the melt pond source contribution. Like the melt pond source, the possible tundra source reduces the overall normalized mean bias (by 14 %) and may contribute to the regional background levels of DMS_g. However, neither source can account for the large unexplained peaks in the measured time series.

ACPD
15, 35547–35589, 2015

4.4.3 Emissions from lakes

To evaluate the potential contribution of DMS from lakes, the fresh water fraction in each GEOS-Chem grid box in a rectangular domain spanning 48 to 75° N and −68 to −140° W was calculated using the Olson Land Cover map, which has a resolution of 1 km. Based on the work of Sharma et al. (1999a), we assigned a mean value of 1 nM DMS to the fresh water in that domain. We then applied the same Liss and Merlivat parameterization as was used to represent the air-water flux for the oceans to the fraction of the grid box with lake coverage. The same caveats apply to the use of transfer velocity parameterizations developed for the open ocean for fluxes from lakes as to the application to melt ponds as discussed above. Under these conditions, the lake source was regionally important as shown in Fig. 6. It resulted in a modest increase in the absolute magnitude of DMS_g in Northern Quebec and Labrador, and had negligible effects elsewhere. The percent change in surface layer DMS_g in the Northwest Territories was quite large due to there being no other sources of DMS_g in that location in GEOS-Chem, but the absolute values of DMS_g are very small. The effect on the simulated DMS_g time series along our ship track in the Arctic is negligible. However, as there are so few measurements of DMS concentrations in lakes in Northern Canada, we cannot exclude the possibility that the actual lake concentrations of DMS_{sw} are much higher than 1 nM and that the unexplained peak in our time series is due to a lake source of DMS_g. This possibility is supported by high chlorophyll-α levels in the lakes of Northern Canada (shown in Fig. S6 in the Supplement) and the fact that the measurements of DMS_{sw} in lakes that we used for this sensitivity test were made more than 15 years ago, and the high northern latitudes have warmed significantly since then (IPCC, 2013).

4.4.4 Emissions from forests and soils

Due to the paucity of measurements of DMS emissions from vegetation, boreal soils, and Arctic wetlands, this potential missing source is by far the most difficult to evaluate. The correlation between the measurement-model residual and the biomass burning

ACPD
15, 35547–35589, 2015

tracers in GEOS-Chem shown in Fig. 4a suggests that the missing DMS was being co-transported with these biomass burning tracers. The measurement-model difference and the MEK tracer have a similar peak on 26 July as shown in Fig. 4a. The FLEXPART-WRF retroplumes (e.g. Period 2 in Fig. 4) identify this time as being continentally influenced.

DMS emissions have been reported from biomass burning (Akagi et al., 2011; Meinardi et al., 2003) and summer 2014 saw a particularly active wildfire season in Northern Canada (Blunden and Arndt, 2015). The simplest reason for the maxima in biomass burning tracers during the unexplained DMS_g peak on 26 July would be emissions of DMS from biomass burning that are not represented in the model. To gauge the importance of this source to DMS_g in the Arctic, we used the emission factor for DMS from boreal forest biomass burning reported by Akagi et al. (2011). We indexed the DMS emissions to CO emissions, such that 3.66×10^{-5} molecules of DMS are emitted for each molecule of CO emitted in GEOS-Chem. Figure 6 shows that the biomass burning sensitivity test showed that the biomass burning source of DMS_g had local influence only, like the modeled lake source. The reason for this is that the emission factor for DMS from boreal forest fires is not very large. As a result, this source acted to increase DMS_g in the immediate vicinity of the wildfires in the Northwest Territories, but had a negligible influence on the time series and is therefore not shown in Fig. 5. The biomass burning source of DMS_g was likely not sufficient to directly influence the DMS_g time series at the ship position, unless the emission factor used in the model is an order of magnitude too low. This seems unlikely as the emission factor we used was derived from direct measurements in a biomass burning plume originating from the boreal forest (Akagi et al., 2011), but remains a possibility as much higher DMS emissions have been measured from other types of biomass burning in other locations (Meinardi et al., 2003).

Further evidence for DMS_g being co-transported with biomass burning tracers is given by improved model-measurement agreement if we assume the biomass burning plume contains equal amounts of DMS_g and MEK, and then add this DMS_g "source"

ACPD
15, 35547–35589, 2015

to the simulated DMS_g. The result of this addition is to decrease the measurement-model bias by 24 % overall, and to reduce the residual by 200 pptv during the 26 July period of interest. The time series of additional DMS_g is shown as the green curve in Fig. 5c. Alternatively, the air mass observed at the ship could have passed over a strong near-land marine source, which is missing in our simulations. The region air mass passed over, however, was nearly entirely ice-covered at the time, making this an unlikely explanation for the observed DMS_g. These results cannot tell us anything about the nature of the continental source, but they highlight the possibility that a source linked in some way to terrestrial flora could have an important effect on DMS_g in the Arctic summer.

Emissions of reduced sulfur species from both soils and lakes are temperature dependent (Bates et al., 1992), opening up the possibility that the wild fires were indirectly promoting DMS emissions. Proximity to wild fires would tend to increase the temperature of the soil as well as changing the quality of the air in a way that might stress biota. A mechanism whereby biomass burning increases the emission of reduced sulfur species such as DMS from soils, lakes and vegetation might yield increased emissions but this requires further study and we do not have any information that would allow implementation of this possible effect in our simulations.

5 Conclusions

Interpreting our recent shipboard DMS_g measurements with the GEOS-Chem chemical transport model, we have shown that local oceanic sources can account for a large proportion (70 %) of the atmospheric surface-layer DMS measured along our ship track in the Canadian Arctic Archipelago and Baffin Bay during summer 2014, and that the ocean was acting as a strong local source of DMS_g. With GEOS-Chem simulations, we have also shown that marine sources south of the Arctic Circle episodically contribute as much as 60 % to DMS mixing ratios in the Canadian Arctic during transport events. The role of transport in controlling DMS levels and the potential for aerosol particle

ACPD
15, 35547–35589, 2015

formation from DMS has been argued convincingly in a global sense by Quinn and Bates (2011). We propose that it may also be important episodically in the Arctic, e.g. transport from the Hudson Bay System or the Northwest Territories. These origins for air at our ship track are also supported by FLEXPART-WRF retroplume analysis.

Overall, source apportionment using FLEXPART-WRF and GEOS-Chem indicate that local sources dominate atmospheric DMS in the Canadian Arctic Archipelago and Baffin Bay. However, GEOS-Chem simulations show a low bias of 67 pptv over the ship track time series (from 10 to 100 % of the measured mixing ratios). We investigated several alternative sources that could act to correct this bias and presented evidence that some of these sources make a non-negligible contribution to surface layer DMS mixing ratios. This included sources from tundra, forests, lakes and melt ponds. Our sensitivity simulations indicated maximum contributions of 6 and 100 % from tundra and melt ponds, respectively, to our DMS_g time series at the ship position, suggesting that emissions of DMS from melt ponds and coastal tundra could have important local, regional effects on DMS levels. Given our confidence in marine-based DMS sources, we also estimated as much as 94 % of the DMS_g at the ship position could be from terrestrial sources (or another source missing from the model) during episodic transport events. These emissions may be related to changes in lake, forest and soil emissions due to the heat and stress associated with biomass burning. Flux measurements from melt ponds and the boreal forest and lakes, particularly when under stress from biomass burning events, are needed to constrain this missing source.

Our findings have implications for our understanding of the sulfur cycle in the summer Arctic and how it has changed in the recent past and will continue to change in the future. For example, much of the discussion surrounding changes in Arctic DMS has focused on the loss of sea ice (Levasseur, 2013), but the loss of permafrost might also have a large impact, by providing nutrients to lakes, for example (Rhüland and Smol, 1998). The potential of the high atmospheric levels of DMS observed during the 2014 campaign to participate in new particle formation and subsequent growth remains to be explored.

ACPD
15, 35547–35589, 2015

The Supplement related to this article is available online at doi:10.5194/acpd-15-35547-2015-supplement.

Acknowledgements. The authors would like to acknowledge the financial support of NSERC for the NETCARE project funded under the Climate Change and Atmospheric Research program. As well, we thank ArcticNet for hosting NETCARE scientists on the Amundsen, in particular the help of Keith Levesque, and all of the crew and scientists aboard. Additionally, special thanks to Amir Aliabadi, Ralf Staebler, Lauren Candlish, Heather Stark, Tonya Burgers and Tim Papakyriakou for ozone sondes and meteorological data. Thanks to Michelle Kim and Tim Bertram of UCSD for invaluable discussions of ion chemistry. The authors thank K. Tavis and P. Kim for their assistance in implementation of the QFED2 database.

References

Akagi, S. K., Yokelson, R. J., Wiedinmyer, C., Alvarado, M. J., Reid, J. S., Karl, T., Crounse, J. D., and Wennberg, P. O.: Emission factors for open and domestic biomass burning for use in atmospheric models, Atmos. Chem. Phys., 11, 4039–4072, doi:10.5194/acp-11-4039-2011, 2011. 35551, 35568

Albrecht, B. A.: Aerosols, cloud microphysics, and fractional cloudiness, Science, 245, 1227–1230, 1989. 35549

Alexander, B., Park, R. J., Jacob, D. J., Li, Q., Yantosca, R. M., Savarino, J., Lee, C., and Thiemens, M.: Sulfate formation in sea-salt aerosols: constraints from oxygen isotopes, J. Geophys. Res.-Atmos., 110, D10307, doi:10.1029/2004JD005659, 2005. 35556

Alexander, B., Park, R. J., Jacob, D. J., and Gong, S.: Transition metal-catalyzed oxidation of atmospheric sulfur: global implications for the sulfur budget, J. Geophys. Res.-Atmos., 114, D02309, doi:10.1029/2008JD010486, 2009. 35556

Allgood, C., Lin, Y., Ma, Y.-C., and Munson, B.: Benzene as a selective chemical ionization reagent gas, Org. Mass Spectrom., 25, 497–502, doi:10.1002/oms.1210251003, 1990. 35553

Bates, T. S., Lamb, B. K., Guenther, A., Dignon, J., and Stoiber, R. E.: Sulfur emissions to the atmosphere from natural sourees, J. Atmos. Chem., 14, 315–337, doi:10.1007/BF00115242, 1992. 35549, 35551, 35569

ACPD
15, 35547–35589, 2015

Bell, T. G., De Bruyn, W., Miller, S. D., Ward, B., Christensen, K. H., and Saltzman, E. S.: Air–sea dimethylsulfide (DMS) gas transfer in the North Atlantic: evidence for limited interfacial gas exchange at high wind speed, Atmos. Chem. Phys., 13, 11073–11087, doi:10.5194/acp-13-11073-2013, 2013. 35560, 35561

Bell, T. G., De Bruyn, W., Marandino, C. A., Miller, S. D., Law, C. S., Smith, M. J., and Saltzman, E. S.: Dimethylsulfide gas transfer coefficients from algal blooms in the Southern Ocean, Atmos. Chem. Phys., 15, 1783–1794, doi:10.5194/acp-15-1783-2015, 2015. 35560, 35561

Bey, I., Jacob, D. J., Yantosca, R. M., Logan, J. A., Field, B. D., Fiore, A. M., Li, Q., Liu, H. Y., Mickley, L. J., and Schultz, M. G.: Global modeling of tropospheric chemistry with assimilated meteorology: model description and evaluation, J. Geophys. Res., 106,23073, doi:10.1029/2001jd000807, 2001. 35556

Blomquist, B. W., Fairall, C. W., Huebert, B. J., Kieber, D. J., and Westby, G. R.: DMS sea-air transfer velocity: direct measurements by eddy covariance and parameterization based on the NOAA/COARE gas transfer model, Geophys. Res. Lett., 33, L07601, doi:10.1029/2006GL025735, doi:10.1029/2006GL025735, 2006. 35558

Blunden, J. and Arndt, D. S.: State of the Climate in 2014, B. Am. Meteorol. Soc., 96, ES1–ES32, doi:10.1175/2015BAMSStateoftheClimate.1, 2015. 35568

Breider, T. J., Mickley, L. J., Jacob, D. J., Wang, Q., Fisher, J. A., Chang, R. Y.-W., and Alexander, B.: Annual distributions and sources of Arctic aerosol components, aerosol optical depth, and aerosol absorption, J. Geophys. Res-Atmos., 119, 4107–4124, doi:10.1002/2013JD020996, 2014. 35556

Brioude, J., Arnold, D., Stohl, A., Cassiani, M., Morton, D., Seibert, P., Angevine, W., Evan, S., Dingwell, A., Fast, J. D., Easter, R. C., Pisso, I., Burkhart, J., and Wotawa, G.: The Lagrangian particle dispersion model FLEXPART-WRF version 3.1, Geosci. Model Dev., 6, 1889–1904, doi:10.5194/gmd-6-1889-2013, 2013. 35555

Browse, J., Carslaw, K. S., Arnold, S. R., Pringle, K., and Boucher, O.: The scavenging processes controlling the seasonal cycle in Arctic sulphate and black carbon aerosol, Atmos. Chem. Phys., 12, 6775–6798, doi:10.5194/acp-12-6775-2012, 2012. 35549

Chang, R. Y.-W., Sjostedt, S. J., Pierce, J. R., Papakyriakou, T. N., Scarratt, M. G., Michaud, S., Levasseur, M., Leaitch, W. R., and Abbatt, J. P. D.: Relating atmospheric and oceanic DMS levels to particle nucleation events in the Canadian Arctic, J. Geophys. Res.-Atmos., 116, D00S03, doi:10.1029/2011JD015926, 2011. 35550, 35582

ACPD
15, 35547–35589, 2015

Charlson, R. J., Lovelock, J. E., Andreae, M. O., and Warren, S. G.: Oceanic phytoplankton, atmospheric sulphur, cloud albedo and climate, Nature, 326, 655–661, doi:10.1038/326655a0, 1987. 35549

Chen, H., Ezell, M. J., Arquero, K. D., Varner, M. E., Dawson, M. L., Gerber, R. B., and Finlayson-Pitts, B. J.: New particle formation and growth from methanesulfonic acid, trimethylamine and water, Phys. Chem. Chem. Phys., 17, 13699—13709, doi:10.1039/C5CP00838G, 2015. 35549

Cole, S. T., Timmermans, M.-L., Toole, J. M., Krishfield, R. A., and Thwaites, F. T.: Ekman veering, internal waves, and turbulence observed under Arctic sea ice, J. Phys. Oceanogr., 44, 1306–1328, doi:10.1175/JPO-D-12-0191.1, 2014. 35559

Croft, B., Martin, R. V., Leaitch, W. R., Tunved, P., Breider, T. J., D'Andrea, S. D., and Pierce, J. R.: Processes controlling the seasonal cycle of Arctic aerosol number and size distributions, Atmos. Chem. Phys. Discuss., 15, 29079–29124, doi:10.5194/acpd-15-29079-2015, 2015. 35556

Darmenov, A. and da Silva, A.: The quick fire emissions dataset (QFED)–documentation of versions 2.1, 2.2 and 2.4, NASA Technical Report Series on Global Modeling and Data Assimilation, NASA TM-2013-104606, 32, 183, 2013. 35556

Duce, R. A., Liss, P. S., Merrill, J. T., Atlas, E. L., Buat-Menard, P., Hicks, B. B., Miller, J. M., Prospero, J. M., Arimoto, R., Church, T. M., Ellis, W., Galloway, J. N., Hansen, L., Jickells, T. D., Knap, A. H., Reinhardt, K. H., Schneider, B., Soudine, A., Tokos, J. J., Tsunogai, S., Wollast, R., and Zhou, M.: The atmospheric input of trace species to the world ocean, Global Biogeochem. Cy., 5, 193–259, doi:10.1029/91GB01778, 1991. 35581

Erickson, D. J., Ghan, S. J., and Penner, J. E.: Global ocean-to-atmosphere dimethyl sulfide flux, J. Geophys. Res.-Atmos., 95, 7543–7552, doi:10.1029/JD095iD06p07543, 1990. 35583

Fairlie, T. D., Jacob, D. J., and Park, R. J.: The impact of transpacific transport of mineral dust in the United States, Atmos. Environ., 41, 1251–1266, 2007. 35556

Fairlie, T. D., Jacob, D. J., Dibb, J. E., Alexander, B., Avery, M. A., van Donkelaar, A., and Zhang, L.: Impact of mineral dust on nitrate, sulfate, and ozone in transpacific Asian pollution plumes, Atmos. Chem. Phys., 10, 3999–4012, doi:10.5194/acp-10-3999-2010, 2010. 35556

Ferland, J., Gosselin, M., and Starr, M.: Environmental control of summer primary production in the Hudson Bay system: the role of stratification, J. Marine Syst., 88, 385–400, doi:10.1016/j.jmarsys.2011.03.015, 2011. 35557

ACPD
15, 35547–35589, 2015

Fisher, J. A., Jacob, D. J., Wang, Q., Bahreini, R., Carouge, C. C., Cubison, M. J., Dibb, J. E., Diehl, T., Jimenez, J. L., Leibensperger, E. M., Lu, Z., Meinders, M. B. J., Pye, H. O. T., Quinn, P. K., Sharma, S., Streets, D. G., van Donkelaar, A., and Yantosca, R. M.: Sources, distribution, and acidity of sulfate-ammonium aerosol in the Arctic in winter-spring, Atmos. Environ., 45, 7301–7318, doi:10.1016/j.atmosenv.2011.08.030, 2011a. 35556

Fisher, J. A., Jacob, D. J., Wang, Q., Bahreini, R., Carouge, C. C., Cubison, M. J., Dibb, J. E., Diehl, T., Jimenez, J. L., Leibensperger, E. M., Lu, Z., Meinders, M. B. J., Pye, H. O. T., Quinn, P. K., Sharma, S., Streets, D. G., van Donkelaar, A., and Yantosca, R. M.: Sources, distribution, and acidity of sulfate–ammonium aerosol in the Arctic in winter–spring, Atmos. Environ., 45, 7301–7318, 2011b. 35556

Fisher, J. A., Jacob, D. J., Soerensen, A. L., Amos, H. M., Steffen, A., and Sunderland, E. M.: Riverine source of Arctic Ocean mercury inferred from atmospheric observations, Nat. Geosci., 5, 499–504, 2012. 35556

Fountoukis, C. and Nenes, A.: ISORROPIA II: a computationally efficient thermodynamic equilibrium model for K^+–Ca^{2+}–Mg^{2+}–NH_4^+–Na^+–SO_4^{2-}–NO_3^-–Cl^-–H_2O aerosols, Atmos. Chem. Phys., 7, 4639–4659, doi:10.5194/acp-7-4639-2007, 2007. 35556

Gries, C., Iii, T. H. N., and Kesselmeier, J.: Exchange of reduced sulfur gases between lichens and the atmosphere, Biogeochemistry, 26, 25–39, doi:10.1007/BF02180402, 1994. 35551, 35566

Hines, M. E. and Morrison, M. C.: Emissions of biogenic sulfur gases from Alaskan tundra, J. Geophys. Res.-Atmos., 97, 16703–16707, doi:10.1029/90JD02576, 1992. 35566

Hopke, P. K., Barrie, L. A., Li, S.-M., Cheng, M.-D., Li, C., and Xie, Y.: Possible sources and preferred pathways for biogenic and non-sea-salt sulfur for the high Arctic, J. Geophys. Res.-Atmos., 100, 16595–16603, doi:10.1029/95JD01712, 1995. 35550, 35564

Huebert, B. J., Blomquist, B. W., Yang, M. X., Archer, S. D., Nightingale, P. D., Yelland, M. J., Stephens, J., Pascal, R. W., and Moat, B. I.: Linearity of DMS transfer coefficient with both friction velocity and wind speed in the moderate wind speed range, Geophys. Res. Lett., 37, L01605, doi:10.1029/2009GL041203, 2010. 35561

IPCC: Summary for policymakers, in: Climate Change 2013: The Physical Science Basis. Contribution of Working Group I to the Fifth Assessment Report of the Intergovernmental Panel on Climate Change, edited by: Stocker, T., Qin, D., Plattner, G.-K., Tignor, M., Allen, S., Boschung, J., Nauels, A., Xia, Y., Bex, V., and Midgley, P., Cambridge University Press, Cambridge, UK and New York, NY, USA, 1–30, 2013. 35567

ACPD
15, 35547–35589, 2015

Jardine, K., Abrell, L., Kurc, S. A., Huxman, T., Ortega, J., and Guenther, A.: Volatile organic compound emissions from *Larrea tridentata* (creosotebush), Atmos. Chem. Phys., 10, 12191–12206, doi:10.5194/acp-10-12191-2010, 2010. 35551

Jardine, K., Yañez-Serrano, A., Williams, J., Kunert, N., Jardine, A., Taylor, T., Abrell, L., Artaxo, P., Guenther, A., Hewitt, C., House, E., Florentino, A. P., Manzi, A., Higuchi, N., Kesselmeier, J., Behrendt, T., Veres, P. R., Derstroff, B., Fuentes, J. D., Martin, S., and Andreae, M. O.: Dimethyl sulfide in the Amazon rain forest, Global Biogeochem. Cy., 2014, GB004969, doi:10.1002/2014GB004969, 2014. 35551

Jeffery, C. D., Robinson, I. S., and Woolf, D. K.: Tuning a physically-based model of the air–sea gas transfer velocity, Ocean Model., 31, 28–35, doi:10.1016/j.ocemod.2009.09.001, 2010. 35559, 35581

Jodwalis, C. M., Benner, R. L., and Eslinger, D. L.: Modeling of dimethyl sulfide ocean mixing, biological production, and sea-to-air flux for high latitudes, J. Geophys. Res.-Atmos., 105, 14387–14399, doi:10.1029/2000JD900023, 2000. 35583

Johnson, M., Hughes, C., Bell, T., and Liss, P.: A Rumsfeldian analysis of uncertainty in air-sea gas exchange, in: Gas Transfer at Water Surfaces, Kyoto University Press, 464–485, 2011. 35561

Johnson, M. T.: A numerical scheme to calculate temperature and salinity dependent air-water transfer velocities for any gas, Ocean Sci., 6, 913–932, doi:10.5194/os-6-913-2010, 2010. 35558, 35559, 35581

Kim, M. J., Zoerb, M. C., Campbell, N. R., Zimmermann, K. J., Blomquist, B. W., Huebert, B. J., and Bertram, T. H.: Revisiting benzene cluster cations for the chemical ionization of dimethyl sulfide and select volatile organic compounds, Atmos. Meas. Tech. Discuss., 8, 10121–10157, doi:10.5194/amtd-8-10121-2015, 2015. 35553

Lana, A., Bell, T. G., Simó, R., Vallina, S. M., Ballabrera-Poy, J., Kettle, A. J., Dachs, J., Bopp, L., Saltzman, E. S., Stefels, J., Johnson, J. E., and Liss, P. S.: An updated climatology of surface dimethlysulfide concentrations and emission fluxes in the global ocean, Global Biogeochem. Cy., 25, GB1004, doi:10.1029/2010GB003850, 2011. 35556, 35557

Leaitch, W. R., Sharma, S., Huang, L., Toom-Sauntry, D., Chivulescu, A., Macdonald, A. M., von Salzen, K., Pierce, J. R., Bertram, A. K., Schroder, J. C., Shantz, N. C., Chang, R. Y.-W., and Norman, A.-L.: Dimethyl sulfide control of the clean summertime Arctic aerosol and cloud, Elementa, 1, 000017, doi:10.12952/journal.elementa.000017, 2013. 35549

ACPD
15, 35547–35589, 2015

Leck, C. and Persson, C.: The central Arctic Ocean as a source of dimethyl sulfide seasonal variability in relation to biological activity, Tellus B, 48, 156–177, doi:10.1034/j.1600-0889.1996.t01-1-00003.x, 1996. 35550, 35582, 35583
Levasseur, M.: Impact of Arctic meltdown on the microbial cycling of sulphur, Nat. Geosci., 6, 691–700, doi:10.1038/ngeo1910, 2013. 35551, 35560, 35565, 35570
Liao, H., Henze, D. K., Seinfeld, J. H., Wu, S., and Mickley, L. J.: Biogenic secondary organic aerosol over the United States: comparison of climatological simulations with observations, J. Geophys. Res.-Atmos., 112, D06201, doi:10.1029/2006JD007813, 2007. 35556
Liss, P.: Processes of gas exchange across an air-water interface, in: Deep Sea Research and Oceanographic Abstracts, vol. 20, Elsevier, 221–238, 1973. 35581
Liss, P. S. and Merlivat, L.: Air-sea gas exchange rates: introduction and synthesis, in: The Role of Air-Sea Exchange in Geochemical Cycling, Springer, 113–127, 1986. 35556, 35559, 35561, 35565, 35581
Lizotte, M., Levasseur, M., Michaud, S., Scarratt, M. G., Merzouk, A., Gosselin, M., Pommier, J., Rivkin, R. B., and Kiene, R. P.: Macroscale patterns of the biological cycling of dimethylsulfoniopropionate (DMSP) and dimethylsulfide (DMS) in the Northwest Atlantic, Biogeochemistry, 110, 183–200, doi:10.1007/s10533-011-9698-4, 2012. 35554
Loose, B., McGillis, W. R., Perovich, D., Zappa, C. J., and Schlosser, P.: A parameter model of gas exchange for the seasonal sea ice zone, Ocean Sci., 10, 17–28, doi:10.5194/os-10-17-2014, 2014. 35559, 35563, 35581
Macdonald, R. W., Kuzyk, Z. A., and Johannessen, S. C.: It is not just about the ice: a geochemical perspective on the changing Arctic Ocean, J. Environ. Sci., 5, 288–301, doi:10.1007/s13412-015-0302-4, 2015. 35551
Mackay, D. and Yeun, A. T.: Mass transfer coefficient correlations for volatilization of organic solutes from water, Environ. Sci. Technol., 17, 211–217, 1983. 35581
Mauritsen, T., Sedlar, J., Tjernström, M., Leck, C., Martin, M., Shupe, M., Sjogren, S., Sierau, B., Persson, P. O. G., Brooks, I. M., and Swietlicki, E.: An Arctic CCN-limited cloud-aerosol regime, Atmos. Chem. Phys., 11, 165–173, doi:10.5194/acp-11-165-2011, 2011. 35550
McGillis, W. R., Dacey, J. W. H., Frew, N. M., Bock, E. J., and Nelson, R. K.: Water-air flux of dimethylsulfide, J. Geophys. Res.-Oceans, 105, 1187–1193, doi:10.1029/1999JC900243, 2000. 35581

ACPD
15, 35547–35589, 2015

Meinardi, S., Simpson, I. J., Blake, N. J., Blake, D. R., and Rowland, F. S.: Dimethyl disulfide (DMDS) and dimethyl sulfide (DMS) emissions from biomass burning in Australia, Geophys. Res. Lett., 30, 1454, doi:10.1029/2003GL016967, 2003. 35551, 35568

Nightingale, P. D., Malin, G., Law, C. S., Watson, A. J., Liss, P. S., Liddicoat, M. I., Boutin, J., and Upstill-Goddard, R. C.: In situ evaluation of air-sea gas exchange parameterizations using novel conservative and volatile tracers, Global Biogeochem. Cy., 14, 373–387, doi:10.1029/1999GB900091, 2000. 35581

Nilsson, E. D. and Leck, C.: A pseudo-Lagrangian study of the sulfur budget in the remote Arctic marine boundary layer, Tellus B, 54, 213–230, doi:10.1034/j.1600-0889.2002.01247.x, 2002. 35550

Nriagu, J. O., Holdway, D. A., and Coker, R. D.: Biogenic sulfur and the acidity of rainfall in remote areas of Canada, Science, 237, 1189–1192, doi:10.1126/science.237.4819.1189, 1987. 35551

Park, R. J., Jacob, D. J., Chin, M., and Martin, R. V.: Sources of carbonaceous aerosols over the United States and implications for natural visibility, J. Geophys. Res.-Atmos., 108, 4355, doi:10.1029/2002JD003190, 2003. 35556

Park, R. J., Jacob, D. J., Field, B. D., Yantosca, R. M., and Chin, M.: Natural and transboundary pollution influences on sulfate-nitrate-ammonium aerosols in the United States: implications for policy, J. Geophys. Res.-Atmos., 109, D15204, doi:10.1029/2003JD004473, 2004. 35556

Park, R. J., Jacob, D. J., Kumar, N., and Yantosca, R. M.: Regional visibility statistics in the United States: natural and transboundary pollution influences, and implications for the Regional Haze Rule, Atmos. Environ., 40, 5405–5423, 2006. 35556

Patris, N., Delmas, R., Legrand, M., De Angelis, M., Ferron, F. A., Stiévenard, M., and Jouzel, J.: First sulfur isotope measurements in central Greenland ice cores along the preindustrial and industrial periods, J. Geophys. Res.-Atmos., 107, ACH 6–1, doi:10.1029/2001JD000672, 2002. 35551

Pirjola, L., Kulmala, M., Wilck, M., Bischoff, A., Stratmann, F., and Otto, E.: Formation of sulphuric acid aerosols and cloud condensation nuclei: an expression for significant nucleation and model comparison, J. Aerosol Sci., 30, 1079–1094, doi:10.1016/S0021-8502(98)00776-9, 1999. 35549

Quinn, P. K. and Bates, T. S.: The case against climate regulation via oceanic phytoplankton sulphur emissions, Nature, 480, 51–56, doi:10.1038/nature10580, 2011. 35570

ACPD
15, 35547–35589, 2015

Rempillo, O., Seguin, A. M., Norman, A.-L., Scarratt, M., Michaud, S., Chang, R., Sjostedt, S., Abbatt, J., Else, B., Papakyriakou, T., Sharma, S., Grasby, S., and Levasseur, M.: Dimethyl sulfide air-sea fluxes and biogenic sulfur as a source of new aerosols in the Arctic fall, J. Geophys. Res.-Atmos., 116, D00S04, doi:10.1029/2011JD016336, 2011. 35550, 35582, 35583

Rhüland, K. and Smol, J. P.: Limnological characteristics of 70 lakes spanning Arctic treeline from Coronation Gulf to Great Slave Lake in the Central Northwest Territories, Canada, Int. Rev. Hydrobiol., 83, 183–203, doi:10.1002/iroh.19980830302, 1998. 35570

Richards, S. R., Rudd, J. W. M., and Kelly, C. A.: Organic volatile sulfur in lakes ranging in sulfate and dissolved salt concentration over five orders of magnitude, Limnol. Oceanogr., 39, 562–572, doi:10.4319/lo.1994.39.3.0562, 1994. 35551

Rosel, A. and Kaleschke, L.: Exceptional melt pond occurrence in the years 2007 and 2011 on the Arctic sea ice revealed from MODIS satellite data, J. Geophys. Res.-Oceans, 117, C05018, doi:10.1029/2011JC007869, 2012. 35551

Scarratt, M. G., Levasseur, M., Schultes, S., Michaud, S., Cantin, G., Vezina, A., Gosselin, M., and De Mora, S. J.: Production and consumption of dimethylsulfide (DMS) in North Atlantic waters, Mar. Ecol.-Prog. Ser., 204, 13–26, 2000. 35554

Shahin, U. M., Holsen, T. M., and Odabasi, M.: Dry deposition measured with a water surface sampler: a comparison to modeled results, Atmos. Environ., 36, 3267–3276, 2002. 35581

Sharma, S., Barrie, L. A., Hastie, D. R., and Kelly, C.: Dimethyl sulfide emissions to the atmosphere from lakes of the Canadian boreal region, J. Geophys. Res.-Atmos., 104, 11585–11592, doi:10.1029/1999JD900127, 1999a. 35551, 35567

Sharma, S., Barrie, L. A., Plummer, D., McConnell, J. C., Brickell, P. C., Levasseur, M., Gosselin, M., and Bates, T. S.: Flux estimation of oceanic dimethyl sulfide around North America, J. Geophys. Res.-Atmos., 104, 21327–21342, doi:10.1029/1999JD900207, 1999b. 35560, 35583

Sharma, S., Chan, E., Ishizawa, M., Toom-Sauntry, D., Gong, S. L., Li, S. M., Tarasick, D. W., Leaitch, W. R., Norman, A., Quinn, P. K., Bates, T. S., Levasseur, M., Barrie, L. A., and Maenhaut, W.: Influence of transport and ocean ice extent on biogenic aerosol sulfur in the Arctic atmosphere, J. Geophys. Res.-Atmos., 117, D12209, doi:10.1029/2011JD017074, 2012. 35550

Simpson, R. M. C., Howell, S. G., Blomquist, B. W., Clarke, A. D., and Huebert, B. J.: Dimethyl sulfide: less important than long-range transport as a source of sulfate to the

ACPD
15, 35547–35589, 2015

remote tropical Pacific marine boundary layer, J. Geophys. Res.-Atmos., 119, 9142–9167, doi:10.1002/2014JD021643, 2014. 35560

Sjostedt, S. J., Leaitch, W. R., Levasseur, M., Scarratt, M., Michaud, S., Motard-Côté, J., Burkhart, J. H., and Abbatt, J. P. D.: Evidence for the uptake of atmospheric acetone and methanol by the Arctic Ocean during late summer DMS-Emission plumes, J. Geophys. Res.-Atmos., 117, D12303, doi:10.1029/2011JD017086, 2012. 35564

Skamarock, W. C., Klemp, J. B., Dudhia, J., Gill, D. O., Barker, D. M., Wang, W., and Powers, J. G.: A description of the advanced research WRF version 2, Tech. rep., DTIC Document, 2005. 35555

Smith, S. R., Bourassa, M. A., and Sharp, R. J.: Establishing more truth in true winds, J. Atmos. Ocean. Tech., 16, 939–952, 1999. 35554

Stohl, A., Forster, C., Frank, A., Seibert, P., and Wotawa, G.: Technical note: The Lagrangian particle dispersion model FLEXPART version 6.2, Atmos. Chem. Phys., 5, 2461–2474, doi:10.5194/acp-5-2461-2005, 2005. 35555

Sweeney, C., Gloor, E., Jacobson, A. R., Key, R. M., McKinley, G., Sarmiento, J. L., and Wanninkhof, R.: Constraining global air-sea gas exchange for CO_2 with recent bomb 14C measurements, Global Biogeochem. Cy., 21, GB2015, doi:10.1029/2006GB002784, 2007. 35581

Tanimoto, H., Kameyama, S., Iwata, T., Inomata, S., and Omori, Y.: Measurement of Air-Sea Exchange of Dimethyl Sulfide and Acetone by PTR-MS Coupled with Gradient Flux Technique, Environ. Sci. Technol., 48, 526–533, doi:10.1021/es4032562, 2013. 35560

Tesdal, J.-E., Christian, J. R., Monahan, A. H., and von Salzen, K.: Sensitivity of modelled sulfate radiative forcing to DMS concentration and air-sea flux formulation, Atmos. Chem. Phys. Discuss., 15, 23931–23968, doi:10.5194/acpd-15-23931-2015, 2015. 35549

Tilling, R. L., Ridout, A., Shepherd, A., and Wingham, D. J.: Increased Arctic sea ice volume after anomalously low melting in 2013, Nat. Geosci., 8, 643–646, doi:10.1038/ngeo2489, 2015. 35549

Tjernström, M., Leck, C., Birch, C. E., Bottenheim, J. W., Brooks, B. J., Brooks, I. M., Bäcklin, L., Chang, R. Y.-W., de Leeuw, G., Di Liberto, L., de la Rosa, S., Granath, E., Graus, M., Hansel, A., Heintzenberg, J., Held, A., Hind, A., Johnston, P., Knulst, J., Martin, M., Matrai, P. A., Mauritsen, T., Müller, M., Norris, S. J., Orellana, M. V., Orsini, D. A., Paatero, J., Persson, P. O. G., Gao, Q., Rauschenberg, C., Ristovski, Z., Sedlar, J., Shupe, M. D., Sierau, B., Sirevaag, A., Sjogren, S., Stetzer, O., Swietlicki, E., Szczodrak, M., Vaatto-

ACPD
15, 35547–35589, 2015

vaara, P., Wahlberg, N., Westberg, M., and Wheeler, C. R.: The Arctic Summer Cloud Ocean Study (ASCOS): overview and experimental design, Atmos. Chem. Phys., 14, 2823–2869, doi:10.5194/acp-14-2823-2014, 2014. 35550, 35582

Twomey, S.: The influence of pollution on the shortwave albedo of clouds, J. Atmos. Sci., 34, 1149–1152, doi:10.1175/1520-0469(1977)034<1149:TIOPOT>2.0.CO;2, 1977. 35549

Wang, Q., Jacob, D. J., Fisher, J. A., Mao, J., Leibensperger, E. M., Carouge, C. C., Le Sager, P., Kondo, Y., Jimenez, J. L., Cubison, M. J., and Doherty, S. J.: Sources of carbonaceous aerosols and deposited black carbon in the Arctic in winter-spring: implications for radiative forcing, Atmos. Chem. Phys., 11, 12453–12473, doi:10.5194/acp-11-12453-2011, 2011. 35556

Wanninkhof, R.: Relationship between wind speed and gas exchange over the ocean, J. Geophys. Res.-Oceans, 97, 7373–7382, doi:10.1029/92JC00188, 1992. 35581

Wanninkhof, R., Asher, W. E., Ho, D. T., Sweeney, C., and McGillis, W. R.: Advances in quantifying air-sea gas exchange and environmental forcing, Annu. Rev. Mar. Sci., 1, 213–244, doi:10.1146/annurev.marine.010908.163742, 2009. 35558

Watts, S. F.: The mass budgets of carbonyl sulfide, dimethyl sulfide, carbon disulfide and hydrogen sulfide, Atmos. Environ., 34, 761–779, doi:10.1016/S1352-2310(99)00342-8, 2000. 35551

Wentworth, G. R., Murphy, J. G., Croft, B., Martin, R. V., Pierce, J. R., Côté, J.-S., Courchesne, I., Tremblay, J.-É., Gagnon, J., Thomas, J. L., Sharma, S., Toom-Sauntry, D., Chivulescu, A., Levasseur, M., and Abbatt, J. P. D.: Ammonia in the summertime Arctic marine boundary layer: sources, sinks and implications, Atmos. Chem. Phys. Discuss., 15, 29973–30016, doi:10.5194/acpd-15-29973-2015, 2015. 35555, 35556

Woolf, D. K.: Bubbles and their role in gas exchange, The Sea, Cambridge University Press, 173–206, 1997. 35581

ACPD
15, 35547–35589, 2015

Table 1. Summary of parameterizations investigated in this work.

	Symbol	Reference	Brief Description	Required Inputs
Air side	D	Duce et al. (1991)	Based on micrometeorology, uses molecular weight of the compound	compound, u
	L	Liss (1973)	Based on data from a wind tunnel study	u
	MY	Mackay and Yeun (1983)	Based on data from a wind tunnel study, uses the Schmidt number of the compound	compound, u, T
	S	Shahin et al. (2002)	Based on data from an in situ study using a surface water sampling device on an urban rooftop, uses the diffusion coefficient of the compound	compound, u, T
	J	Jeffery et al. (2010); Johnson (2010)	NOAA COARE fully physically based model, modified here to fit better with observations	compound, u, T
Water side	W	Wanninkhof (1992)	Global estimate based on bomb ^{14}C inventory	compound, T, u, S
	L	Liss and Merlivat (1986)	Lake experiments using SF_6 and wind tunnel observations	compound, T, u, S
	S	Sweeney et al. (2007)	Global estimate based on bomb ^{14}C inventory	compound, T, u, S
	N	Nightingale et al. (2000)	Deliberate multi-tracer study (considered the state of the art)	compound, T, u, S
	W97	Woolf (1997)	Physically based, includes compound-specific bubble effect	compound, T, u, S
	M	McGillis et al. (2000)	Cubit fit to field data	compound, T, u, S
	Lo	Loose et al. (2014)	Fully physically based, includes effects of sea ice. Only valid in regions with non-zero sea ice coverage	T, u, S, u_{ice}, ice concentration

Johnson (2010)'s R implementation was used for the first 11. Loose et al. (2014)'s Matlab implementation was used for the last parameterization (FJLo, including the effect of sea ice). Flux estimates are named in figures by the letter F followed by the symbol shown in this table for the air-side and water-side parameterization.

ACPD
15, 35547–35589, 2015

Table 2. Summary of past DMS mixing ratio measurements in the Arctic.

Study	Leck and Persson (1996)	Rempillo et al. (2011)	Rempillo et al. (2011)	Chang et al. (2011)	Tjernström et al. (2014)	This Work
Cruise Name	IAOE-91	Amundsen 2007	Amundsen 2008	Amundsen 2008	ASCOS 2008	Amundsen 2014
Season	Fall (Aug, Sep, Oct)	Fall (Early Oct)	Fall (Late Sep)	Fall (End of Aug, Sep)	Fall (Aug, beginning of Sep)	Summer (Late Jul and Early Aug)
Location	Central Arctic Ocean	Western Canadian Arctic	Eastern Canadian Arctic	Eastern Canadian Arctic	Central Arctic Ocean	Eastern Canadian Arctic
Method	Gas chromatography	Gas chromatography	Gas chromatography	Proton Transfer Reaction Mass Spectrometry	Proton Transfer Reaction Mass Spectrometry	Benzene Chemical Ionization Mass Spectrometry
Measurement Frequency	392 samples in 64 days	9 samples in 3 days	18 samples in 3 days	5 min	1 min	10 Hz
Median	25 (1.1)	10 (0.44)	30 (1.3)	65.9	26	185.8
25th percentile	11 (0.48)			41.2	15	117.8
75th percentile	53 (2.3)			98.9	50	262.5
Minimum	1.1 (0.047)	Below detection (< 7 pptv)	Below detection (< 7 pptv)	0.3	4.0	Below detection (< 4 pptv)
Maximum	380 (17)	30 (1.3)	94 (4.1)	474	158	1155

The studies of Leck and Persson (1996) and Rempillo et al. (2011) report concentrations in nmol m^{-3}. For purposes of comparison, these have been converted to mixing ratios for an atmospheric pressure and temperature of 101 kPa and 4° respectively. Original (published) concentration values are reported in parentheses following the calculated mixing ratios.

ACPD
15, 35547–35589, 2015

Table 3. Summary of previous air-ocean DMS flux values in the Arctic.

Flux	Date	Location	Method	Authors
0.02–12 μmol m^{-2} d^{-1}	Summer 2014 (Jul and Aug)	Eastern Canadian Arctic	Estimated from measurements	This work
0.1–2.6 μmol m^{-2} d^{-1}	Fall 2007, 2008 (Sep to Nov)	Beaufort Sea to Baffin bay through Lancaster Sound	Estimated from measurements	Rempillo et al. (2011)
0.002–8.4 μmol m^{-2} d^{-1}	Fall 1991 (Aug to Oct)	Central Arctic Ocean and Greenland Sea	Estimated from measurements	Leck and Persson (1996)
0.007–11.5 μmol m^{-2} d^{-1}	Summer 1994 (Jul and Aug)	Central Arctic Ocean East–West transect	Estimated from measurements	Sharma et al. (1999b)
0.5 μmol m^{-2} d^{-1}	Jan	North of 60° N	Global model	Erickson et al. (1990)
4–12 μmol m^{-2} d^{-1}	Mar–Dec 1996	Gulf of Alaska	Regional Model	Jodwalis et al. (2000)

ACPD
15, 35547–35589, 2015

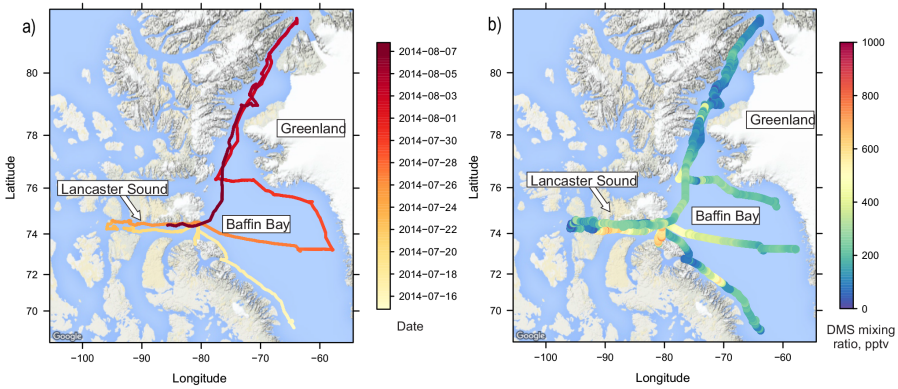

Figure 1. (a) The Amundsen ship position with dates indicated by colours. **(b)** Surface-layer atmospheric dimethyl sulfide (DMS) mixing ratios from ship-based high resolution time of flight chemical ionization mass spectrometer (HR-ToF-CIMS) measurement with colour showing magnitude of mixing ratios.

ACPD
15, 35547–35589, 2015

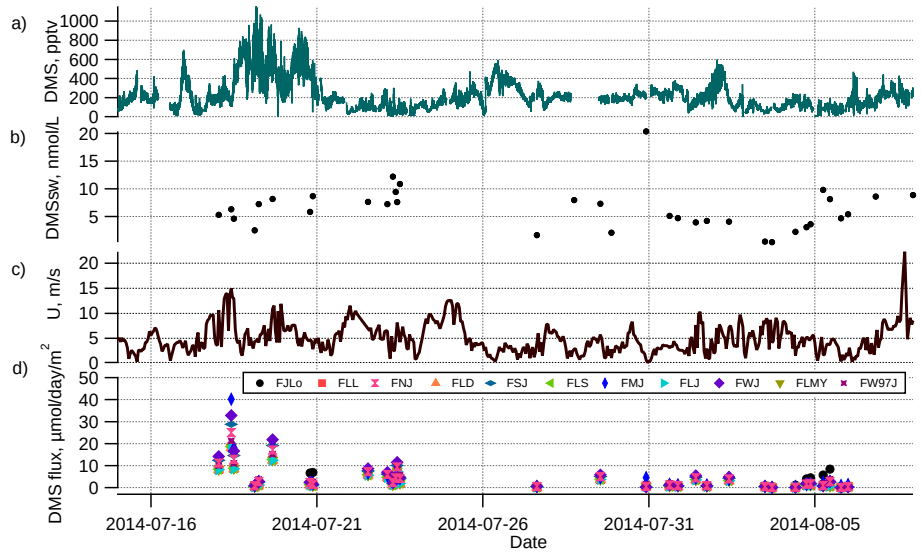

Figure 2. Time series along Amundsen ship track of **(a)** atmospheric DMS mixing ratio (10 Hz) from HR-ToF-CIMS, **(b)** observed DMS surface seawater concentration, **(c)** hourly-averaged wind speed at ship position, **(d)** DMS water-air flux estimates for all choices of transfer velocity parameterization (symbol acronyms explained in Table 1 footnotes).

ACPD
15, 35547–35589, 2015

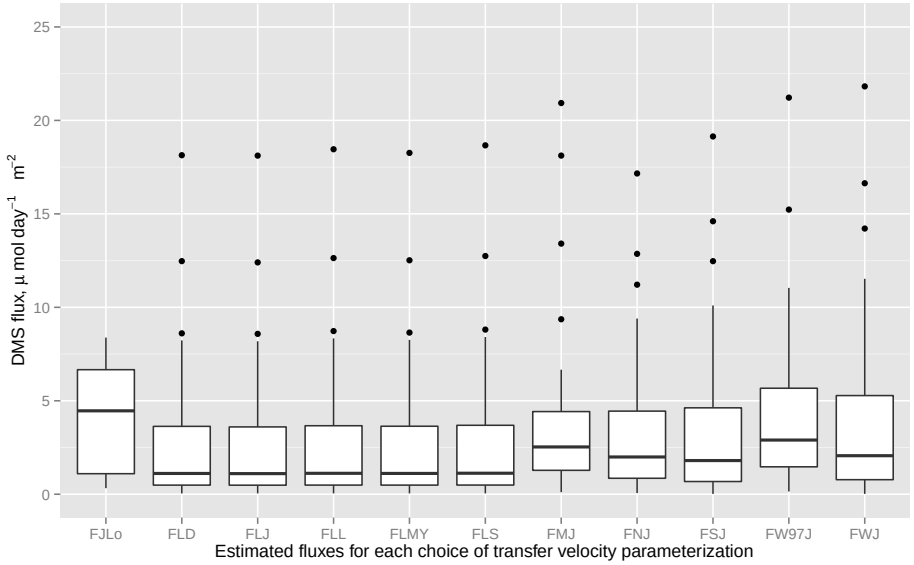

Figure 3. Regional median DMS flux estimates for all choices of transfer velocity parameterization (symbol acronyms explained in Table 1 footnotes). The middle line of the box shows the median. The top and bottom box edges show the upper and lower quartiles (1/4 and 3/4 of the data, respectively). The whiskers show the maximum and minimum values, excluding outliers, which are represented by single points. Outliers differ from the upper and lower quartiles by more than a factor of 1.5.

ACPD
15, 35547–35589, 2015

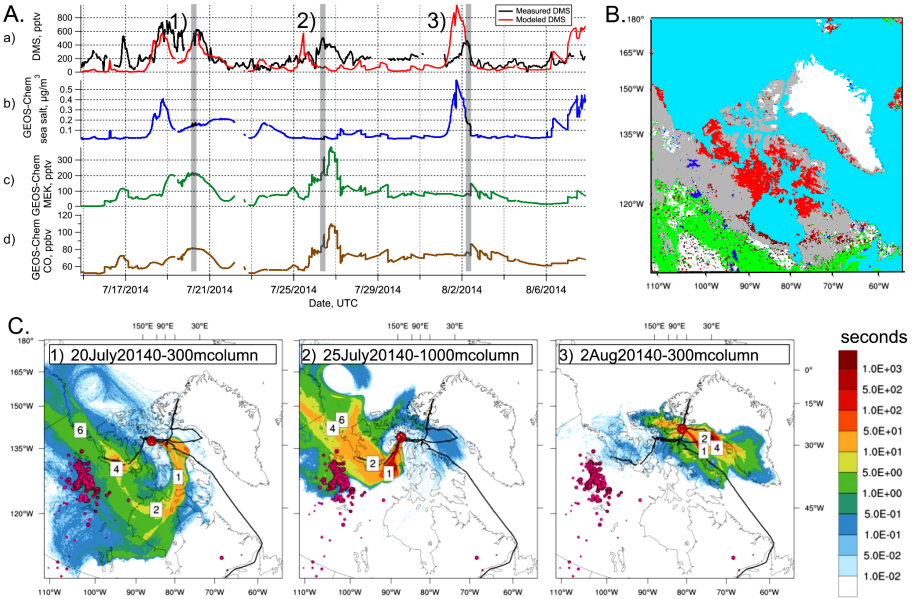

Figure 4. Panel **(a)** Surface-layer atmospheric time series along Amundsen ship track of **(a)** measured and GEOS-Chem (GC) simulated DMS, **(b)** GC simulation of accumulation mode sea salt mass concentration, **(c)** GC simulation of methyl ethyl ketone (MEK) mixing ratio, **(d)** GC simulation of carbon monoxide (CO) mixing ratio. Panel **(b)** Olson Land Cover map of North America showing low-lying tundra (red), other tundra (gray), forest (green), wetlands and marsh (brown) and inland water (dark blue). Panel **(c)** FLEXPART-WRF potential emissions sensitivity (PES) simulation plots showing the likely origin of the air mass at the ship position. The colour scale in seconds corresponds to time spent in the lower 300–1000 m (marked on each plot) before arriving at the ship position. The three plots correspond to the three periods shown by the numbers and shaded bars in Panel **(a)**, showing examples of (1) transport from lower latitudes, including Hudson Bay (2) continentally influenced air (3) local marine influence from Baffin Bay.

ACPD
15, 35547–35589, 2015

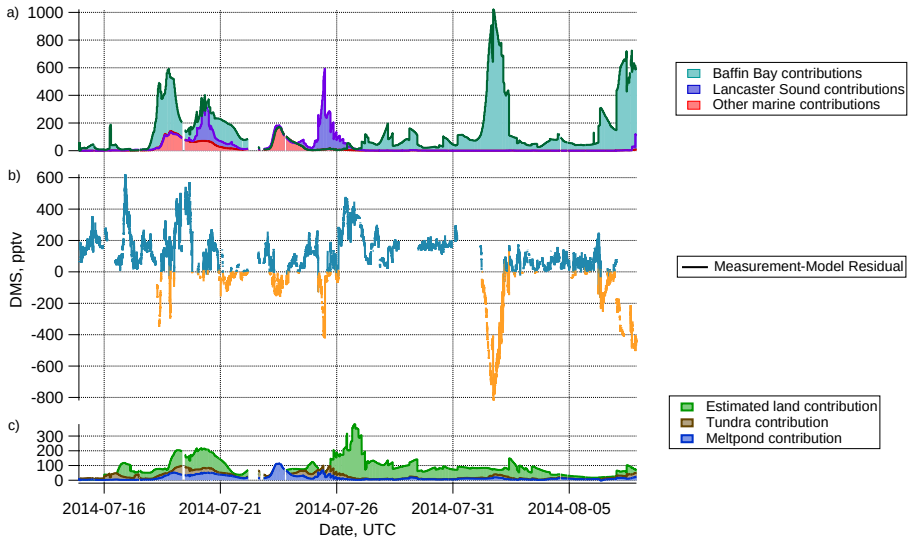

Figure 5. (a) GEOS-Chem (GC) simulated of atmospheric surface-layer DMS mixing ratio along Amundsen ship track as in Fig. 4a, with indication of contributions from Baffin Bay (blue), from Lancaster Sound (purple), and from other marine regions (red). **(b)** Difference between measurement and simulated DMS mixing ratio time series along the ship track showing model over prediction in blue and under prediction in orange. **(c)** GC simulated DMS contributions along ship track from sensitivity tests for additional DMS sources such as melt ponds (blue), tundra (brown), and unknown terrestrial (forests, soils, lakes)/near-terrestrial marine sources (green).

ACPD
15, 35547–35589, 2015

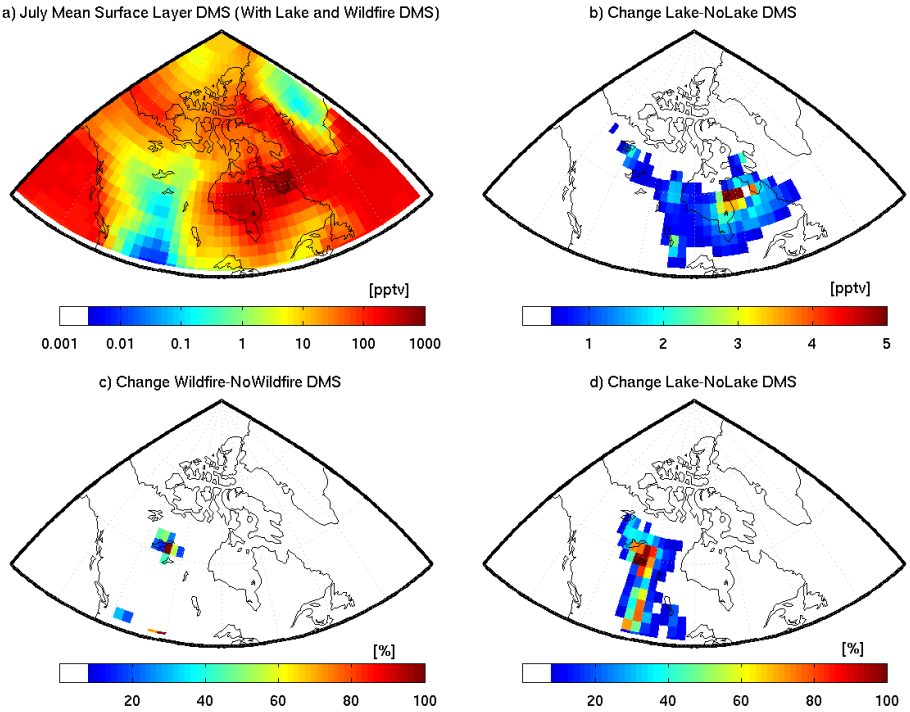

Figure 6. (a) GEOS-Chem simulated July mean surface-layer atmospheric DMS in Canada, **(b)** absolute change in simulated surface layer DMS with implementation of lake DMS emissions, **(c)** percent change in simulated Canadian surface layer DMS due to DMS emissions from wildfires, **(d)** percent changes in simulated surface layer DMS with the implementation of lake DMS emissions.

ACPD
15, 35547–35589, 2015